Journal of Applied Fluid Mechanics, Vol. 14, No. 3, pp. 741-752, 2021.
Available online at www.jafmonline.net, ISSN 1735-3572, EISSN 1735-3645.
DOI: 10.47176/jafm.14.03.31933

Film Cooling Performance of the Staggered Arrangement of Auxiliary Holes and Main Holes on a Flat Plate

W. Zhang[1,2†] and H. R. Zhu[1]

[1]*School of Power and Energy, Northwestern Polytechnical University, Xi'an，Shaanxi Province, 710072, China*
[2]*School of Aero-engine, Shenyang Aerospace University, Shenyang, Liaoning Province, 110136, China*

†*Corresponding Author Email: emma7691@163.com*

(Received June 23, 2020; accepted November 2, 2020)

ABSTRACT

The film cooling effectiveness of a staggered arrangement of small and large holes was investigated. The small auxiliary holes were located normal to the cooled surface, whereas the large main holes had an inclination angle of 30°. The center points of the small holes were located upstream, downstream, and in the same position as the main holes. A hole pitch (P/D) of 3 and a thickness (t/D) of 3 were considered. The film cooling performance of the hole in trench structure and the cylindrical hole was also determined. The numerical results show that large-scale vortices caused by the auxiliary hole injection inhibit the development of vortices caused by the main hole in the streamwise direction. This result differs from that of anti-vortex film cooling. Compared to the baseline, the increase in the surface-averaged values is 15-22% for the staggered arrangement, depending on the blowing ratio (0.5 to 2.0). The positions of the auxiliary holes have an effect on the spanwise-averaged values.

Keywords: Turbine; Film effectiveness; Vortex inhibition.

NOMENCLATURE

ave	averaged
aw	adiabatic wall
c	coolant
d	diameter of auxiliary hole
D	diameter of main hole
l	large main film hole
L	length of hole
loc	location of hole outlet without film
M	blowing ratio
m	mass flow rate of the fluid
P	spanwise pitch of neighboring main hole
Re	Reynolds number
s	small auxiliary film hole
sur	cooled surface
T	temperature
t	thickness of the film hole plate
Tu	turbulence intensity
u	flow velocity
x	streamwise distance from the main hole center
y	cooled surface-normal direction
z	spanwise distance
ρ	density
θ	dimensionless temperature
η	film cooling effectiveness
β	inclination angle of auxiliary hole
α	inclination angle of main hole
∞	mainstream

1. INTRODUCTION

Film cooling is typically applied on the turbine blades of aerospace engines to ensure normal operation under high turbine inlet temperatures. Cool air from the compressor is supplied to the bladed. A substantial effort was carried out to provide sufficient cooling. A reduction in the ejection angle brought down the aerodynamic loss coefficient at the blade exit and also improved the effectiveness (Babu *et al*. 2020). The coolant leaves the blade surface due to counter-rotating vortices, leading to the bad cooling performance. It is believed that holes with expanded exits improve the film coverage because of the decreased exit momentum flux. Several studies on film cooling of

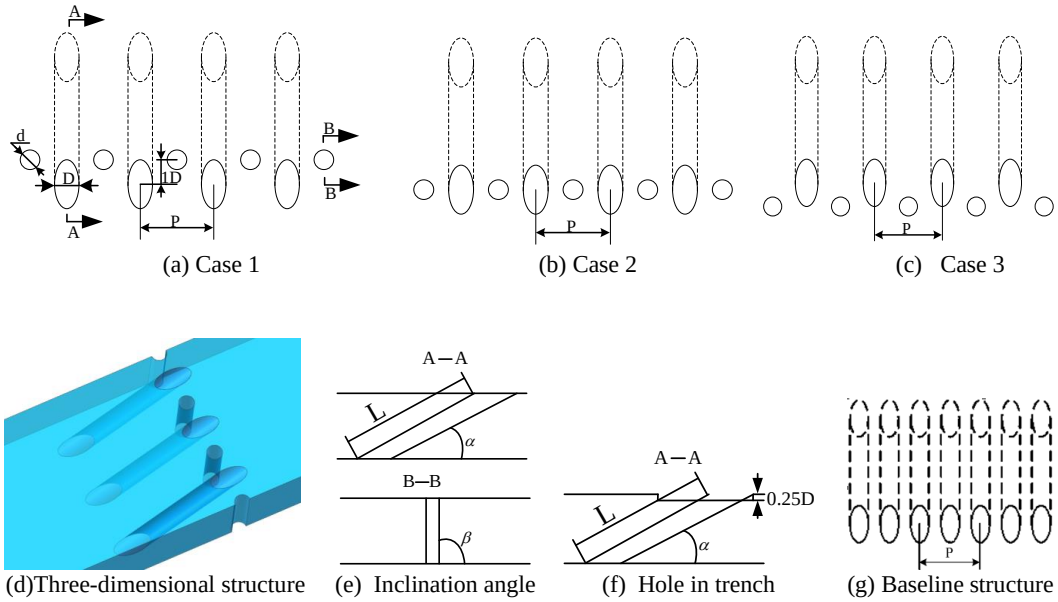

(a) Case 1 (b) Case 2 (c) Case 3

(d)Three-dimensional structure (e) Inclination angle (f) Hole in trench (g) Baseline structure

Fig. 1. Film hole structures.

expanded holes were published in the last two decades (Gritsch *et al*. 1998; Yusop *et al*. 2013; James *et al*. 2008; Willam *et al*. 2008). The optimal blow ratio of expanded holes has been increased. Will *et al*. (2011) studied the relationship between the effectiveness and the injection angle, coverage ratio, hole pitch, downstream distance, and blowing ratio for different hole shapes. The dual-fan hole was also used to analyze the effect of the hole inlet shape (Bai *et al*. 2009; Li *et al*. 2008; Li *et al*. 2017). It was found that a higher discharge coefficient of the dual-fan hole resulted in a slight change in the effectiveness. Increasing the injection angle increased the effectiveness near the film hole but also resulted in a high heat transfer coefficient. Christian and Achmed (2012) analyzed the cooling performances of laidback holes, laidback fan holes, and conical holes. Converging slot-holes provided improved film performance because of the accelerated flow and the continuous spanwise spread inside the film hole (Sargison *et al*. 2002; Pu *et al*. 2015; Liu *et al*. 2011a; Yao *et al*. 2014). The author proposed using an upstream ramp and downstream micro-tamp vortex generator to increase the effectiveness (Na and Shih 2007; Shinn and Vanka 2013). Abdala *et al*. (2016; 2015) assessed the effect of upstream steps, including one normal step and four curve steps. It was observed that a relatively narrow curve step provided the better film performance. Zheng *et al*. (2017) investigated the effects of divided steps. Seven coolant delivery configurations were designed to eliminate kidney vortex. (Jiang *et al*. 2021). An anti-vortex was observed in film cooling by Heidmann and Ekkad (2008). The authors found that a suitable percentage of the mass flow through the branch holes was crucial to improving the film performance. The film performance for six anti-vortex holes with different branch hole diameters and exit locations was further studied by Dhungel *et al*. (2009) and Christopher *et al*. (2013). Salimi *et al*. (2016) studied the effects of adding another cooling port upstream of the main jet. A significant film cooling improvement was observed. Numerical simulations were conducted to determine the effect of using one inlet and two outlets hole (Li *et al*. 2018). This structure required round holes, which are easy to fabricate. However, it was difficult to ensure that the center axes of the three cylindrical holes intersected at one point; the film performance was sensitive to the location of the branch hole. Moreover, the sharp corners produced by joining the neighboring holes caused stress concentration. The application of this configuration is limited. The objectives of this work are as follows:

(1) to propose a novel, simple, and effective cooling concept using a staggered arrangement of large inclined main holes and small auxiliary holes; both are cylindrical holes.

(2) to conduct a coupling analysis of the thermal field and flow field to clarify the mechanism of vortex cancellation.

(3) to analyze the effect of the auxiliary hole location on the effectiveness.

2. FILM HOLE GEOMETRY

Figure 1 shows the geometrical structures of the holes with the staggered arrangement and the baseline structure. The only difference between the three structures is the auxiliary hole positions. In case 2, the exit center of the auxiliary holes is the same as that of the large holes. In cases 1 and 3, the distances are 1 diameter (D) upstream and 1 D downstream of the large hole exit, respectively. A three-dimensional view for case 2 is provided. The typical main hole pitch (P/D=3) and the thickness (t/D=3) are considered. The auxiliary holes with diameters of 0.8 times that of the main holes are located halfway between the neighboring main

Table 1 Hole geometries

Geometries	*L/D*	*d/D*	*P/D*	*t/D*	α	β	Location of the center of the auxiliary hole exit
Case 1	6	0.8	3	3	30°	90°	1 *D* upstream of the large hole exit center
Case 2	6	0.8	3	3	30°	90°	the same *x/D* as the main hole exit center
Case 3	6	0.8	3	3	30°	90°	1 *D* downstream of the large hole exit center
Hole in trench	6	/	3	3	30°	/	/
Baseline	6	/	3	3	30°	/	/

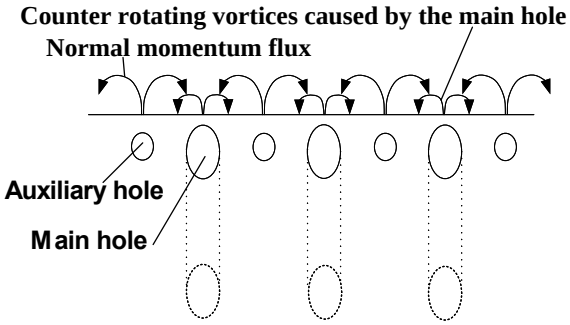

Fig. 2. Potential flow downstream of the holes with a staggered arrangement.

holes. The number of baseline holes is the same as the total number of holes with a staggered arrangement, and the diameter is 0.906D to ensure the same flowing cross-section area of the baseline hole and the staggered hole rows. Therefore, all the structures have the same mass flow of the coolant. The flowing cross-sectional areas of the main hole, auxiliary hole, and baseline hole are 12.56, 8.03, and 10.29 mm^2, respectively. The dimensionless geometrical parameter of the baseline structure depends on the main hole diameter. The pitch is defined as the distance between two holes. The same inclination angle of 30° for the main hole and the baseline hole is considered. The hole-in-trench structure with a depth of 0.25 D and the same cylindrical hole parameter is presented as a comparison. The hole geometry are listed in Table 1. As shown in Fig. 2, since the auxiliary hole has a relatively large normal momentum flux, the induced auxiliary vortices inhibit the counter-rotating vortices caused by the main hole flowing onto the cooled surface, thereby the improved film performance downstream.

3. COMPUTATIONAL METHOD

3.1 Grids of Computational Domain

The staggered arrangement domain is shown in Fig. 3. It included one main hole, two halves of the auxiliary hole, and one plenum. The height of the mainstream tunnel was 10 times the main hole diameter to ensure that the coolant injection was not influenced by the wall. The plenum with 10D×10D×3D was large enough for the coolant. The unstructured and the structured grids were respectively generated in the middle region and in the other regions for the mainstream tunnel. The grid was very dense around the hole exit to get the interaction of the coolant jet and the mainstream. A similar grid point distribution and density for the different cases were maintained to facilitate the comparison. The size of the first-layer grid was 0.002 mm, resulting in the y+ values to be less than 1. The grid size increased by a factor of 1.2 with increasing distance from the cooled surface.

The grid independence analysis was based on case 2. Three numbers of meshes were examined (2.2×10^6, 3.1×10^6, and 4.1×10^6 nodes). Figure 4 shows the spanwise averaged effectiveness values for the different grid numbers at M=1.0. An increase in the grid number from 2.2×10^6 to 3.1×10^6 increased the relative difference by 4-12%. The results were similar for an increase in the number of grids from 3.1×10^6 to 4.1×10^6, indicating that the mesh with 3.1×10^6 nodes was appropriate for the calculation. The same grid number was also used in the calculation of the other cases.

3.2 Simulation Method and Convergence

The realizable k-e turbulence model with the modified turbulent Prandtl number was used, which provides higher accuracy (Liu *et al*. 2011b). The SIMPLE algorithm and the second-order upwind differences were used. The normalized residuals were less than 10^{-5} at convergence. A point (x/D=4, y/D=0.5, z/D=0) was selected for the analysis. Figure 5 shows the change in the velocity at this point during the iteration. When the iteration number reached 1000, the velocity stabilized, indicating convergence.

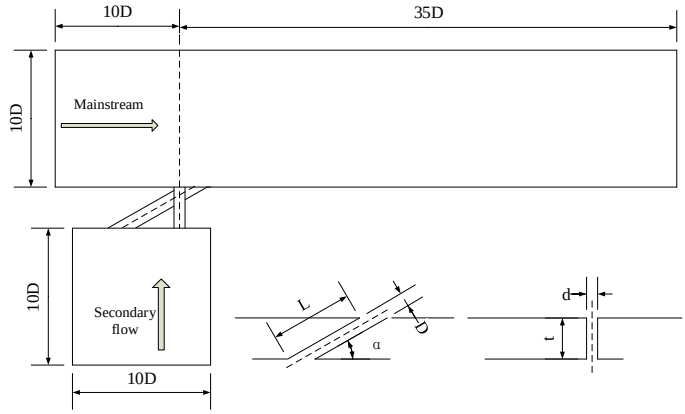

(a) Two-dimensional sketch

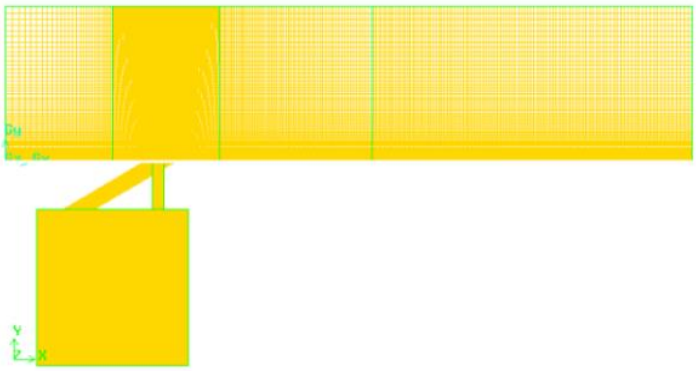

(b) Computational domain

Fig. 3. Computational domain and grids.

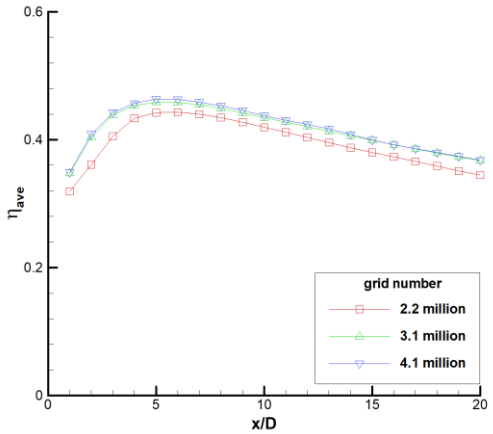

Fig. 4. Grid independence analysis.

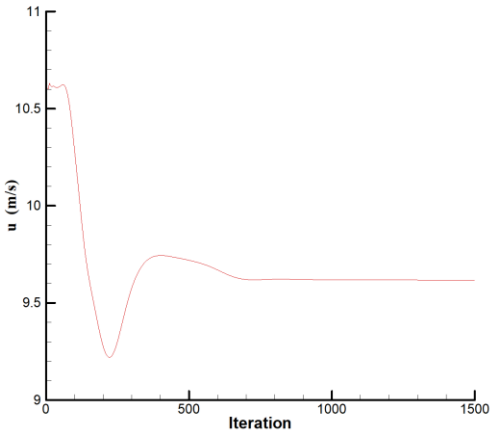

Fig. 5. Convergence of the calculation analysis.

3.3 Parameter Definitions and Boundary Conditions

The blowing ratio was calculated using Eq. (1):

$$M=\rho_c u_c / \rho_{loc} u_{loc}=\left(\frac{\dot{m}_l+\dot{m}_s}{A_l+A_s}\right)/\rho_{loc} u_{loc} \tag{1}$$

where A_l and A_s are the area of the large hole and the auxiliary hole cross-section, respectively. $\dot{m}_l$ and $\dot{m}_s$ are the averaged mass flow rate of the two holes.

The spanwise averaged film effectiveness was obtained by Eq. (2):

$$\eta_{ave}=\frac{\int_{-1.5}^{1.5}\eta d(\frac{z}{D})}{3} \tag{2}$$

The surface averaged film effectiveness was calculated by Eq. (3)

$$\eta_{sur\_ave}=\frac{\int_{0}^{20}\int_{-1.5}^{1.5}\eta d(\frac{z}{D})d(\frac{x}{D})}{20\times 3} \tag{3}$$

A velocity magnitude was given by 15 m/s at the mainstream tunnel inlet, leading to the Reynolds number of 6500, whose characteristic length was based on the main hole diameter. The changes in the pressure and the temperature were very small in this experiment; thus, constant properties were acceptable. The mainstream temperature was 300 K. The inlet of the plenum providing the coolant had different mass flow rates. The sidewalls had the periodic boundary. The coolant temperature was 270 K. The turbulence intensities at both inlets were set by 1%.

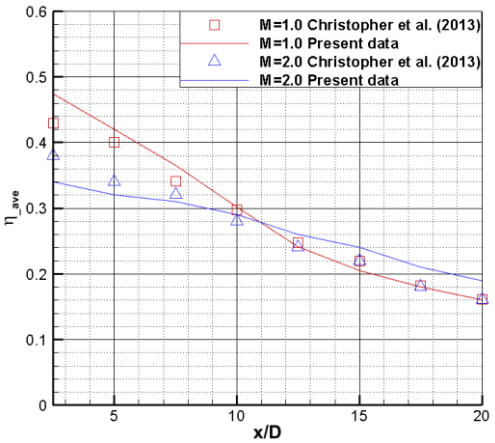

Fig. 6. Comparison of the spanwise averaged effectiveness.

4. RESULTS AND DISCUSSION

4.1 Validation of the code

According to the result of the grid independence test, a grid with 3.1×10^6 nodes was used. Figure 6 shows the spanwise averaged values obtained by Christopher *et al.* (2013) and in this study for M=1.0 and 2.0. The same film hole geometries were used. A good agreement was found.

4.2 Flow Characteristics

The cooling performance improvement depends on the jet interaction of the normal small auxiliary hole and the large main hole; thus, an analysis of the vortices is performed first. Figure 7 displays the streamline and dimensional temperature on the x/D=4 plane, which is normal to the main stream direction for the four structures. All the distances are normalized by the main hole diameter. The values of one spanwise period is presented. For the baseline, the well-known vortex pair is observed. The vortex center is about 0.45 D from the wall, leading to a large increase in the temperature of the coolant near the cooled wall. The main hole jet keeps closer to the wall for cases 1, 2, 3 than the baseline. Meanwhile, the vortex from the large hole jet, which is responsible for the weak film cooling, is reduced. The vortices formed by the injection of the auxiliary hole ensure that the jets of the large hole remain attached to the wall for case 1 and 2 which have similar flows and temperature distributions. In case 3, the jet from the main hole is not compressed on the surface as in case 1 and 2; however, the center of the vortices from the side auxiliary hole is much closer to the wall than in case 1 and 2, ensuring good cooling downstream of the auxiliary hole.

Case 2 is selected to study the blowing ratio effect on the flow and temperature distribution. Figures 8-11 show the vortices and the dimensionless temperature for case 2 at all the studied blowing ratios. The characteristics of the vortices depend on the blowing ratios. Inhibited vortices different from the anti-vortex are observed in the present study. At M=0.5, four vortices, such as the case of the standard cylindrical hole row, are observed due to the weak interaction between the large and small holes. An increase in the blowing ratio to 1.0 increases the scales of the auxiliary vortices. At x/D=6, the main counter-rotating vortices have been significantly inhibited. A further increase causes the relatively large auxiliary vortices to suppress the main counter-rotating vortices on the cooled surface, inhibiting the development of the main counter-rotating vortices in the streamwise direction. This result indicates that the auxiliary hole injection is more effective at high blowing ratios. The long penetration distance of the jet out of the auxiliary hole indicates low utilization of the coolant but results in improved attachment of the jet from the main hole, thereby improving the cooling performance. The coolant remains attached to the cooled surface because the auxiliary hole injection inhibits the vortices when increasing the blowing ratio.

4.3 Film Cooling Effectiveness

Figure 12 displays the spanwise averaged values of the four structures. The origin of the x-coordinate is located at the center of the main hole exit. At M=0.5, the values of the staggered arrangement is lower than that of the baseline in x/D<7 region, and the effect is more pronounced for case 3. The differences in the mass flow rates and the very weak interactions between the large and the small holes shown in Fig. 8 lead to the non-uniform spanwise film coverage. This result indicates that the standard small hole results in low values at a low blowing ratio. At M=1.0, 1.5, and 2.0, the values of all staggered arrangement are higher, and the effect is more pronounced in x/D<5 region. The largest increase (0.1) occurs at x/D=5 and is attributed to the auxiliary vortices, which inhibit the development of the main counter-rotating vortices, as shown in Figs. 7, 9, 10, and 11. Moving the auxiliary hole from upstream to downstream primarily affects the region within x/D<5. The values near the film hole decreases by 60% and is less than 10% at x/D=1 and 5 respectively when the auxiliary hole is moved from upstream to downstream. This result shows that the values near

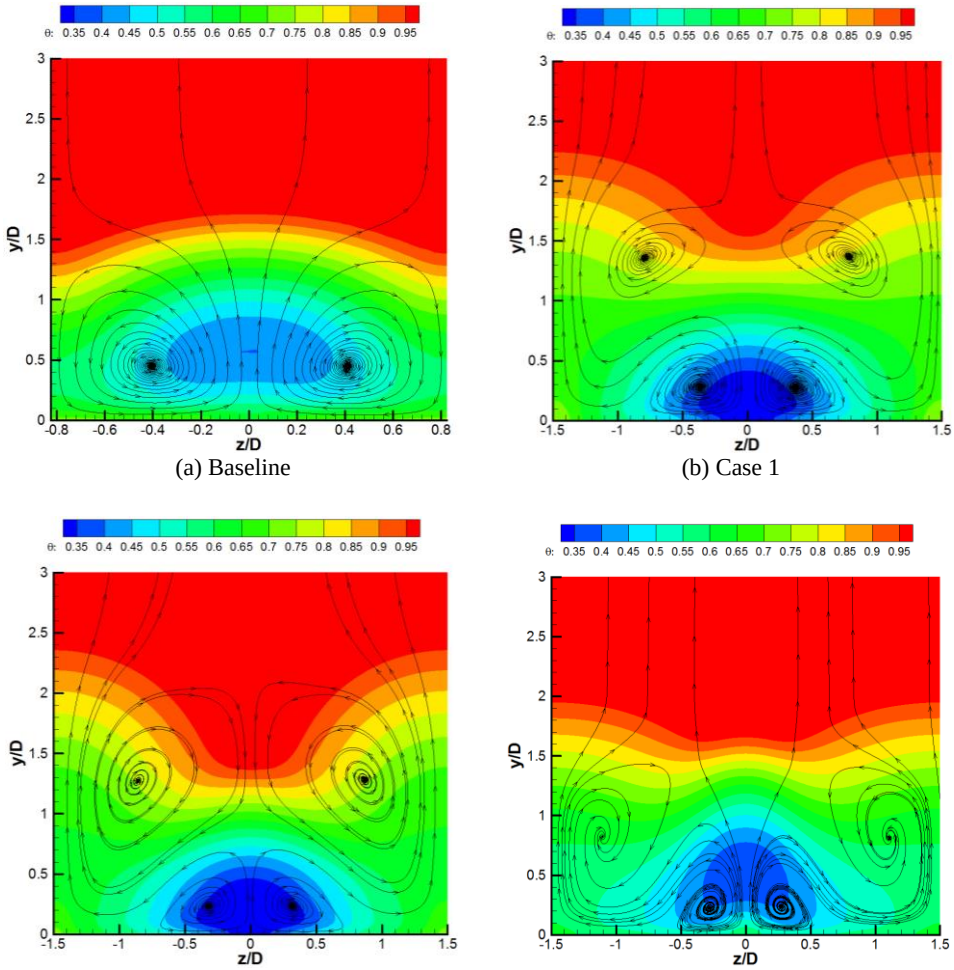

(a) Baseline (b) Case 1

(c) Case 2 (d) Case 3

Fig. 7. Streamlines and the dimensionless temperature for the four structures at M=1.5.

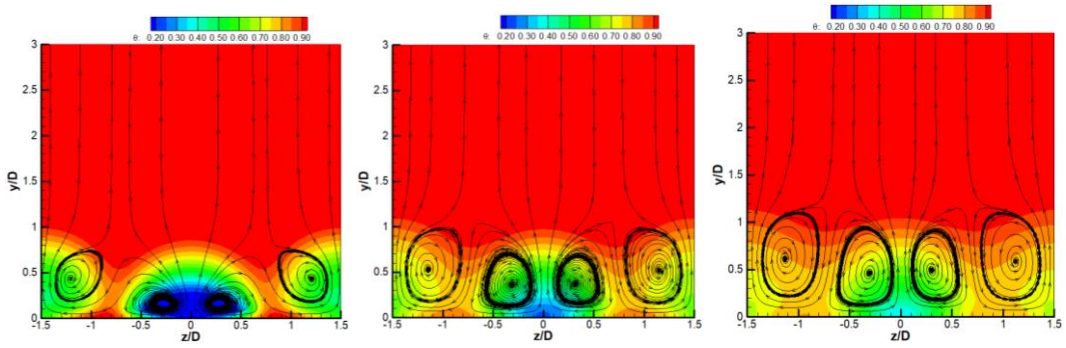

(a) x/D=2 (b) x/D=4 (c) x/D=6

Fig. 8. Streamlines and the dimensionless temperature for the staggered arrangement of case 2 at M=0.5.

the hole is sensitive to the streamwise location of the small hole. In the x/D>5 region, the value difference is less than 8% for the three staggered arrangements.

Figure 13 displays the distributions of the spanwise values at x/D=4. An increase of the blowing ratio at the centerline of z/D=0 decreases the effectiveness values by 0.38 for the baseline and by less than 0.1 for the staggered arrangement due to the weak separation of the main hole injection. The blowing ratio effect at z/D=±1.5 is relatively small. This result demonstrates that an increase in the coolant through the auxiliary hole improves the coverage of the film through the main hole. There is the similar spanwise distributions for case 1 and 2. Case 3 has a much more uniform spanwise distribution than the other two cases. At M=0.5, similar spanwise distributions are observed for the four structures, with three peaks and two troughs. The distribution is more uniform for the staggered arrangement case at the other three blowing ratios.

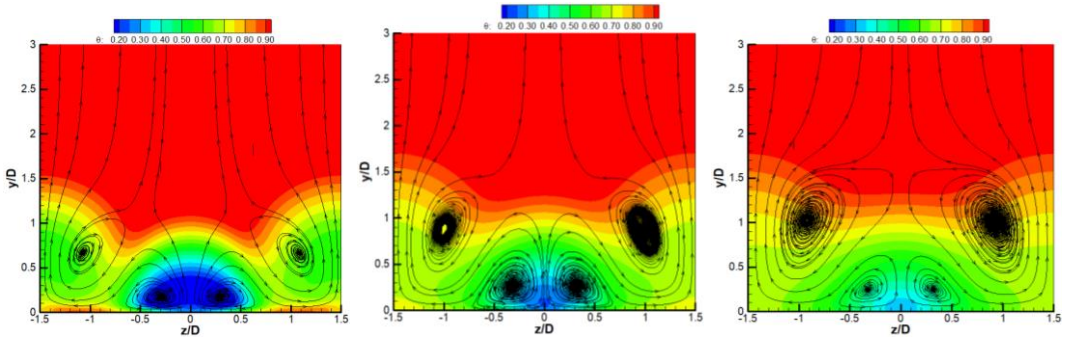

(a) x/D=2 (b) x/D=4 (c) x/D=6

Fig. 9. Streamlines and the dimensionless temperature for the staggered arrangement of case 2 at M=1.0.

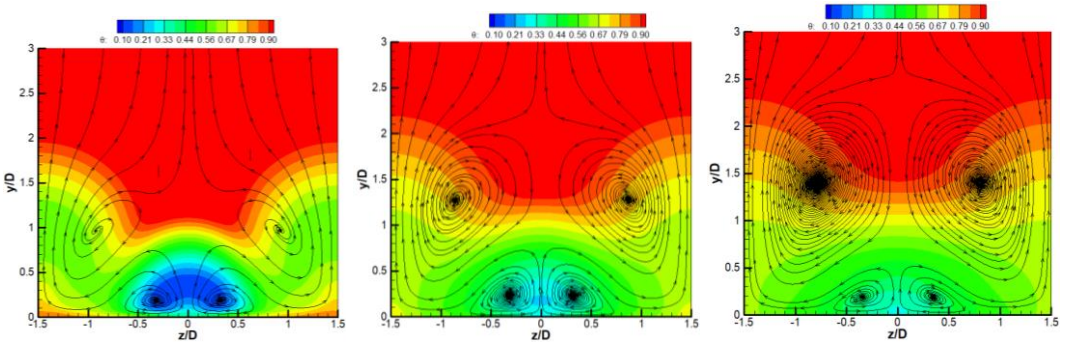

(a) x/D=2 (b) x/D=4 (c) x/D=6

Fig. 10. Streamlines and the dimensionless temperature for the staggered arrangement of case 2 at M=1.5.

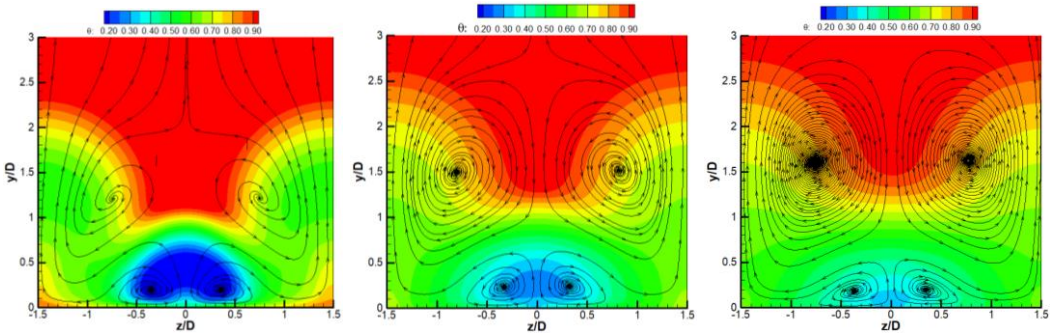

(a) x/D=2 (b) x/D=4 (c) x/D=6

Fig. 11. Streamlines and the dimensionless temperature for the staggered arrangement of case 2 at M=2.0.

Figure 14 shows the hole geometry effect at the centerline. At M=0.5, the values for the staggered arrangement of the cases 1 and 2 are similar and somewhat higher than the baseline. The values for case 3 are lower than those of the baseline in x/D<8 region. At M=1.0 and 1.5, the values of case 1 and 2 are higher than that of the baseline because of the better attachment. At M=2.0, the values are highest for case 1 at x/D=10. With an increase of the x/D, the differences between the three cases decrease, but the values are higher than those of the baseline.

Figure 15 shows the surface averaged values of the four structures. The values of the baseline and the staggered arrangements increase with an increase of the blowing ratio. It is noteworthy that some of the gas enters the sublayer of the coolant due to the relatively small hole pitch of the baseline structure, resulting in higher values. At M=0.5, there is a slight difference of about 0.03. At the other three blowing ratios, the staggered arrangements have similar values, which are 15-22% higher than the baseline values. Figure 16 shows the local values on the surface in one spanwise period for the four structures at different blowing ratios. A region of very high values occurs near the main hole exit in case 1. This result indicates good coverage of the coolant on the surface as it is ejected from the main hole. A region of high values (> 0.6) is observed in case 1 and 2. Case 3 has a much more uniform distribution in the spanwise direction than the other cases. The uniformity of the spanwise coverage improves with an increase of the blowing ratio.

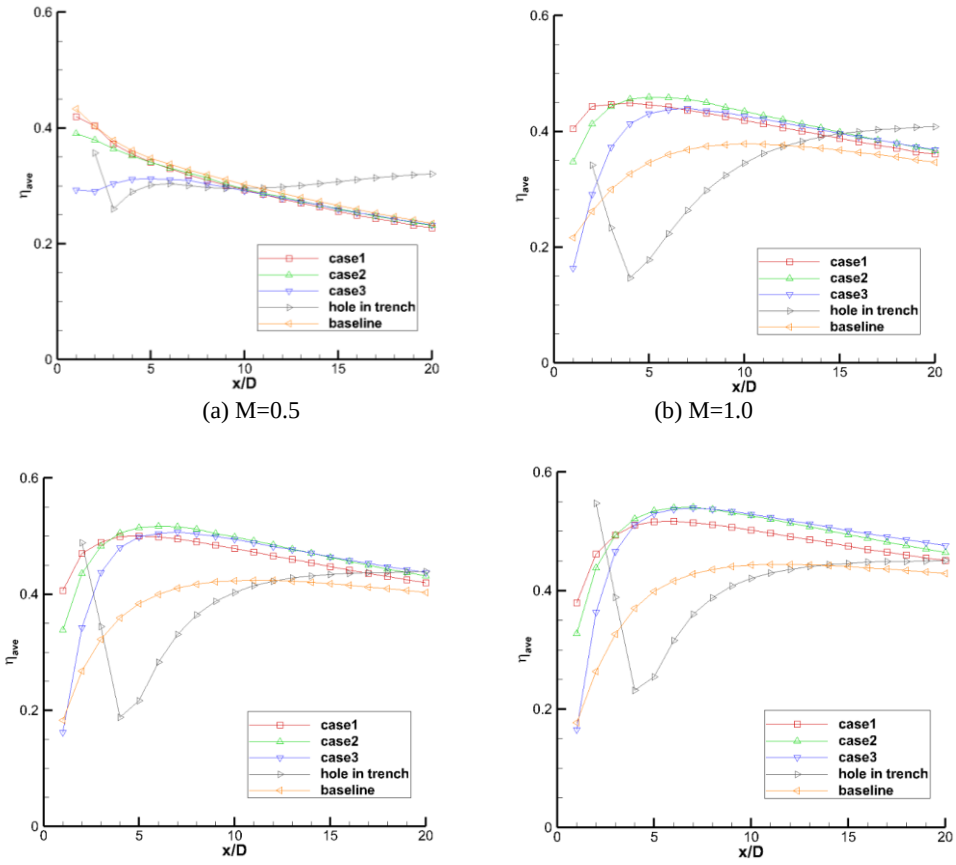

(a) M=0.5 (b) M=1.0

(c) M=1.5 (d) M=2.0

Fig. 12. Effect of the hole geometry on the spanwise averaged effectiveness.

Figure 17 shows the percentage of the total mass flow through the main hole. According to published data of the anti-vortex hole, the percentage for optimum effectiveness is about 64.2%. The percentages of the mass flow through the main holes in this study range from 57% to 62%, depending on the position of the auxiliary holes. This finding demonstrates that the proposed structures provide a reasonable percentage of the mass flow through the auxiliary holes to inhibit the development of counter-rotating vortices.

4. CONCLUSION

A novel and simple staggered arrangement consisting of separate round holes was proposed to improve the film performance. The distribution of the values and the vortices were obtained from a numerical simulation. The important findings of this study are as follows:

(1) The large auxiliary vortices inhibited the main counter-rotating vortices development in the streamwise direction. The vortices formed by the injection of the auxiliary hole ensured that the jets remained close to the wall. Meanwhile, the size and strength of the kidney vortex from the large hole jet was reduced. The ability to inhibit the vortices improved with the blowing ratio increasing.

(2) Compared to the baseline, the staggered arrangement of the cylindrical holes significantly increased the values except for the x/D<1 region for case 3. Moving the auxiliary hole from upstream to downstream primarily affected the x/D<5 region. The value decreased by 60% at x/D=1 and by less than 10% at x/D=5.

(3) The surfaced averaged values were similar for the three staggered structures. Compared to the baseline, the increase in the surface averaged values was 15-22%, depending on the blowing ratio (0.5 to 2.0). The uniformity of the spanwise effectiveness improved with the blowing ratio increasing.

(4) The small hole geometry effect, such as the hole diameter, injection angle, and hole pitch, should be further investigated. The larger main hole pitch effect also requires further study to improve the applicability to vanes or blades. The heat transfer coefficient for the staggered arrangement between the small and large cylindrical holes requires additional analysis.

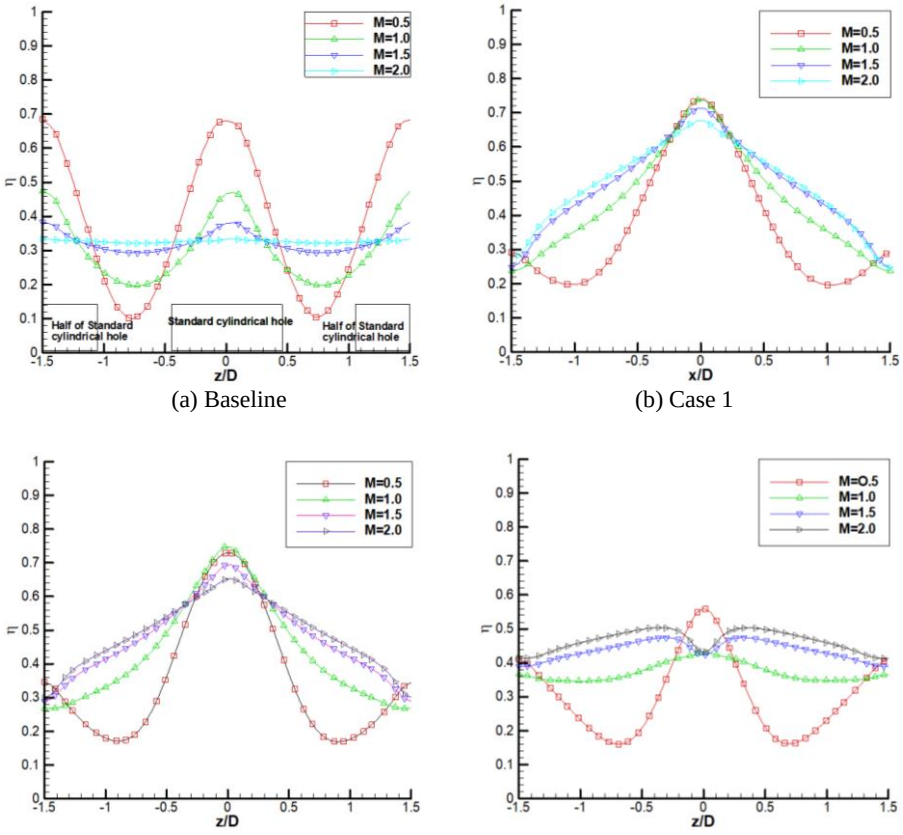

(a) Baseline (b) Case 1

(c) Case 2 (d) Case 3

Fig. 13. Spanwise distribution of the effectiveness.

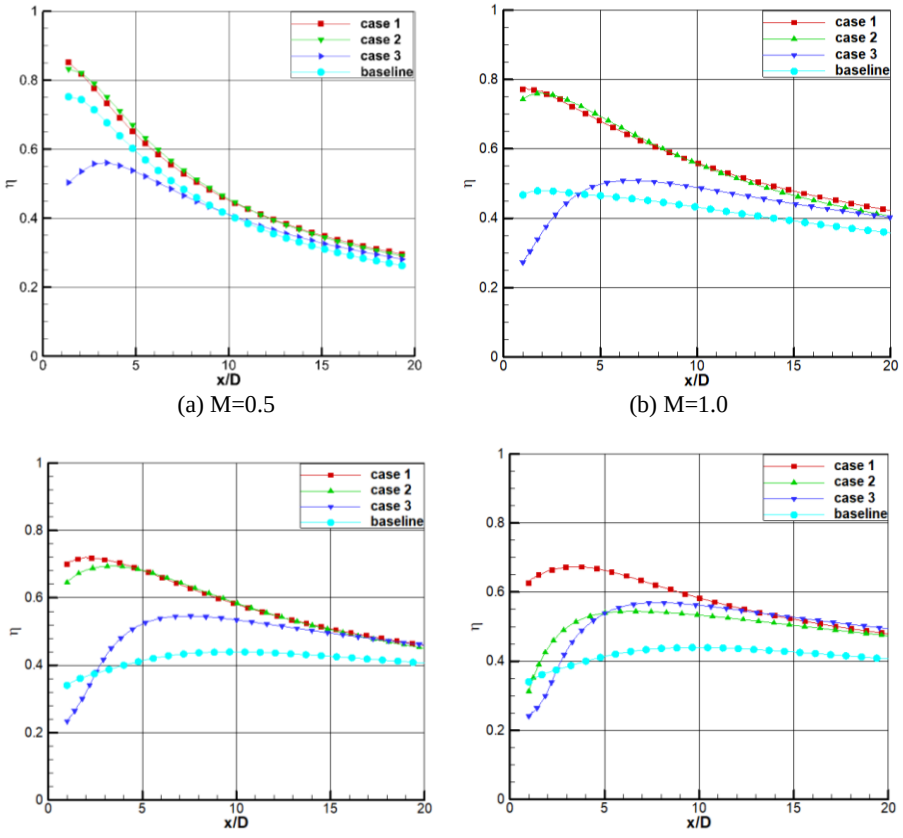

(a) M=0.5 (b) M=1.0

(c) M=1.5 (d) M=2.0

Fig. 14. Effectiveness at the center line.

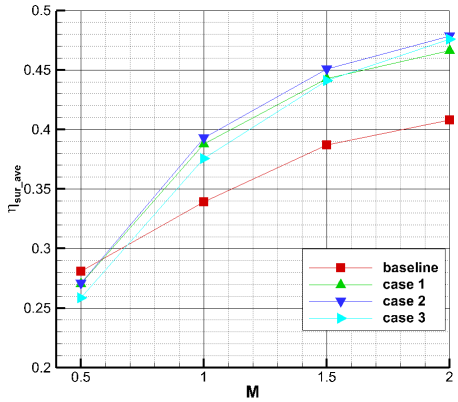

Fig. 15. Surface averaged effectiveness.

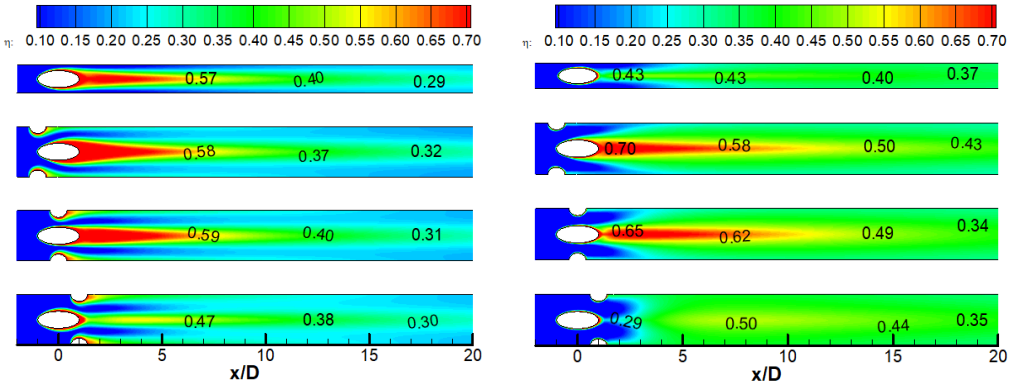

(a) M=0.5

(b) M=1.0

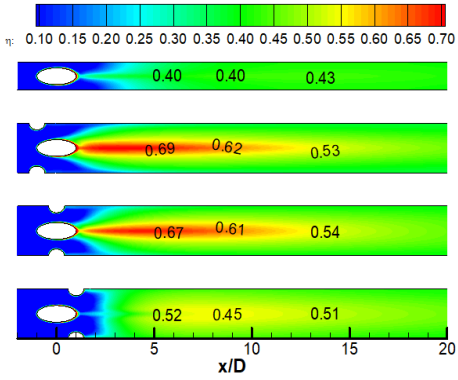

(c) M=1.5

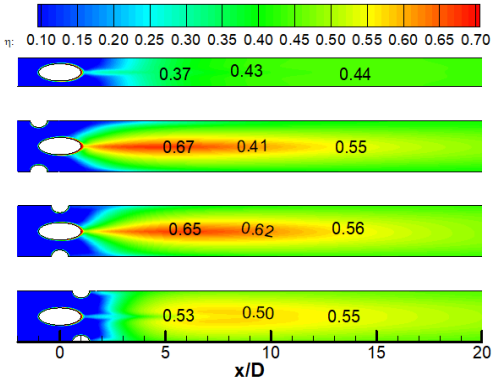

(d) M=2.0

Fig. 16. Two-dimensional distribution of the effectiveness.

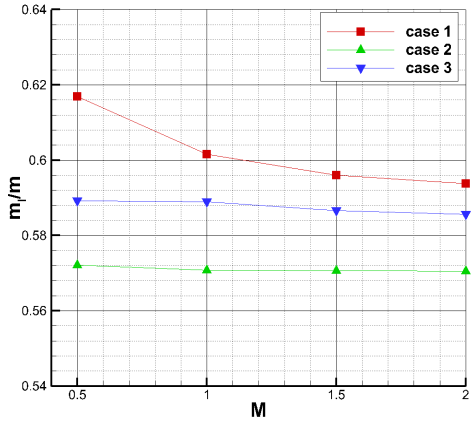

Fig. 17. Percentage of mass flow through the main hole.

REFERENCES

Abdala, A. M. M. and F. N. M. Elwekeel (2016). An influence of novel upstream steps on film cooling performance. *International Journal of Heat and Mass Transfer* 93(Feb.), 86-96.

Abdala, A. M. M., F. N. M. Elwekeel and D. Huang (2015). Film cooling effectiveness and flow structures for novel upstream steps. *Applied Thermal Engineering* 105 (May.), 1-14.

Babu, S. and S. Anish (2020). Computational Predictions of Velocity Ratio and Ejection Angle on Purge Flow in a Linear Turbine Cascade with Upstream Disturbance. *Journal of Applied Fluid Mechanics* 14 (1), 335-347.

Bai, J. T., H. R. Zhu and C. L. Liu (2009, June). Film cooling characteristic of double-fan-shape film cooling holes. Proceedings of the 54th ASME Turbo Expo 2009, Orlando, Florida, USA, 185-198.

Christian, S. and S. Achmed (2012). Effect of geometry variations on the cooling performance of fan-shaped cooling holes. *Journal of Turbomachinery* 134(6), 061008.

Christopher, L., D. P. Narzary and S. Ekkad (2013). Film-cooling performance of antivortex hole on a flat plate. *Journal of Turbomachinery* 135(3), 061009(1-11).

Dhungel, A., Y. Lu, W. Phillips, S. V. Ekkad and J. Heidmann (2009). Film cooling from a row of holes supplemented with antivortex holes. *Journal of Turbomachinery* 131(2), 1-10.

Gritsch, M., A. Schulz A and S. Wittig (1998). Adiabatic wall effectiveness measurements of film-cooling holes with expanded exits. *Journal of Turbomachinery* 120(3), 549-556.

Heidmann, J. D. and S. Ekkad (2008). A novel antivortex turbine film-cooling hole concept. *Journal of Turbomachinery* 130(3), 031020-031028.

James, S. P., J. E. Sargison, G. J. Walker and A. D. Henderson (2008). A comparative investigation of round and fan-shaped cooling hole near flow fields. *Journal of Turbomachinery* 130, 041020(1-8).

Jiang, Y. T., H. F. Deng, X. L. You, H. J. Zhao and G. Q (2021). Yue. Numerical Investigation on Film Cooling Mechanism with Different Coolant Delivery Configurations. *Journal of Applied Fluid Mechanics* 14 (1), 175-185.

Li , G. C., H. F. Wang, W. Zhang, Z. H. Kou and R. S. Xu (2017). Film cooling performance of a row of dual-fanned holes at various injection angles. *Journal of Thermal Science* 26 (5), 453-458.

Li, G. C., H. R. Zhu and H. Fan (2008). Influence of hole shape on film cooling characteristics with co2 injection. *Chinese Journal of Aeronautics* 21(5), 462-471.

Li, G. C., Y. K. Chen, Z. H. Kou, W. Zhang and G. C. Zhang (2018). Mechanism of film cooling with one inlet and double outlet hole injection at various turbulence intensities. I*nternational Journal of Turbo & Jet-Engines* 135(1), 1-9.

Liu, C. L., H. R. Zhu and J. T. Bai (2011a). Film cooling performance of converging-slot holes with different exit-entry area ratios. *Journal of Turbomachinery* 133(1), 011020.

Liu, C. L., H. R. Zhu and J. T. Bai (2011b). New development of the turbulent Prandtl number models for the computation of film cooling effectiveness. *International Journal of Heat and Mass Transfer* 54 (4), 874–886.

Na, S. and T. I. P. Shih (2007). Increasing adiabatic film-cooling effectiveness by using an upstream ramp. *Journal of Heat Transfer* 129(4), 464-471.

Pu, J., J. Wang, S. Ma and X. Wu (2015). An experimental investigation of geometric effect of upstream converging slot-hole on end-wall film cooling and secondary vortex characteristics. *Experimental Thermal and Fluid Science* 69(Agu.), 58-72.

Salimi, M. R., M. Ramezanizadeh, M. Taeibi-Rahni and R. Farhadi-Azar (2016). Film Cooling Effectiveness Enhancement Applying another Jet in the Upstream Neighbor of the Main Jet-Using LES Approach. *Journal of Applied Fluid Mechanics* 9(1), 33-42.

Sargison, J. E., S. M. Guo, M. L. G. Oldfield, G. D. Lock and A. J. Rawlinson (2002). A converging slot-hole film-cooling geometry—Part 2: transonic nozzle guide vane heat transfer and loss. *Journal of Turbomachinery* 124(3), 461-471.

Shinn, A. F. and S. P. Vanka (2013). Large eddy simulations of film-cooling flows with a micro-ramp vortex generator. *Journal of Turbomachinery* 135(1), 1-13.

Will, F. C., A. T. Karen and B. David (2011). A film-cooling correlation for shaped holes on a flat-plate surface. *Journal of Turbomachinery* 133(1), 011002(1-11).

Willam, R. S. and G. B. David (2015). Experimental thermal field measurements of film cooling above the suction surface of a turbine vane. *Journal of Engineering for Gas Turbines and Power* 137(10), 102604(1-10).

Yao, Y., J. Zhang and X. Tan (2014). Numerical study of film cooling from converging slot-hole on a gas turbine blade suction side. *International communications on heat and mass transfer* 52(Jan.), 61-72.

Yusop, N. M., A. H. Ali and M. Z. Abdullah

(2013). Computational study of a new scheme for a film-cooling hole on convex surface of turbine blades. *International Communications in Heat and Mass Transfer* 43 (Fub.), 90-99.

Zheng, D. R., X. J. Wang, F. Zhang and Q. Yuan (2017). Numerical investigation on the effects of the divided steps on film cooling performance. *Applied Thermal Engineering* 124(Jun.), 652-662.